ACS APPLIED MATERIALS & INTERFACES

Research Article

www.acsami.org

Theoretical Study of H_2O Adsorption on Zn_2GeO_4 Surfaces: Effects of Surface State and Structure–Activity Relationships

Li Liu,[†,‡] Xian Zhao,[§] Honggang Sun,[§] Chuanyi Jia,[§] and Weiliu Fan*[,†]

[†]School of Chemistry and Chemical Engineering and [§]State Key Laboratory of Crystal Materials, Shandong University, Jinan 250100, China

[‡]School of Light Chemistry and Environment Engineering, Qilu University of Technology, Jinan 250353, China

Supporting Information

ABSTRACT: We employed the density functional theory to investigate the interaction of H_2O with Zn_2GeO_4 surfaces, considering both perfect and defective surfaces. The results revealed that the interaction of H_2O with Zn_2GeO_4 surfaces was dependent on the structure of the latter. For perfect surfaces, H_2O adsorbed at the $Ge_{3c}\cdots O_{2c}$ site of a (010) surface could spontaneously dissociate into an H atom and an OH group, whereas H_2O tended to adsorb at the O_{2c}-M_{3c}-O_{3c} site of a (001) surface by molecular adsorption. The presence of oxygen defects was found to strongly promote H_2O dissociation on the (010) surface. Analysis of the surface electronic structure showed a large density of Ge states at the top of the valence band for both perfect and defective (010) surfaces, which is an important factor affecting H_2O dissociation. In contrast, perfect and defective (001) surfaces with surface Ge states buried inside the valence band were significantly less reactive, and H_2O was adsorbed on these surfaces in the molecular form. This information about the adsorbate geometries, catalytic activity of various surface sites, specific electronic structure of surface Ge atoms, and their relevance to surface structure will be useful for the future design of the Zn_2GeO_4 photocatalyst, as well as for the atomistic-level understanding of other structure-sensitive reactions.

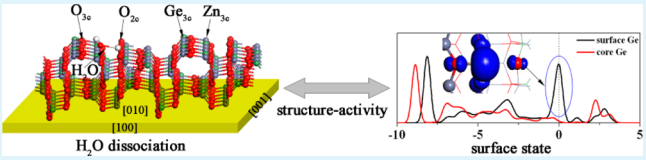

KEYWORDS: *density functional theory, H_2O adsorption, Zn_2GeO_4, photocatalysis, surface state, structure–activity relationships*

1. INTRODUCTION

Semiconductor photocatalytic reactions are typically surface-based processes, and the photocatalytic efficiency is dependent on morphology, microstructure, and surface properties of semiconductor materials participating in the reactions.[1−6] In recent years, notable progress has been made in the shape-controlled synthesis of photocatalytic materials and investigation of the relationship between their morphological or structural characteristics and photocatalytic properties.[1,7−9] However, only a few theoretical calculations describing how the surface structure of photocatalysts affect their properties have been reported. A theoretical understanding of the influence of photocatalysts' surface structure and identification of the active sites involved in the photocatalytic process are extremely important for the design and synthesis of novel photocatalysts.

Zinc orthogermanate (Zn_2GeO_4)—an important wide-bandgap semiconductor photocatalyst—has shown high activity for water splitting and degradation of organic pollutants.[10,11] Recently, it has been found that Zn_2GeO_4 nanobelts when used as photocatalysts greatly improve the photocatalytic activity toward the reduction of CO_2 into CH_4 in the presence of water vapor.[11] This reaction is an eight-electron process and consists of a sequence of steps involving electron and proton transfers, C−O bond breaking, and C−H bond formation.[12] The mechanism of this reaction is more complicated than that of a simple reaction. Therefore, the theoretical study of the interactions of Zn_2GeO_4 with CO_2 and H_2O separately is important. In our previous work, we studied CO_2 adsorption on perfect and defective Zn_2GeO_4 surfaces and concluded that the interaction of CO_2 with Zn_2GeO_4 surfaces is dependent on the surface structure.[13] In addition, we found that the major exposed perfect (010) surfaces of Zn_2GeO_4 nanobelts did not display the highest activity for CO_2 activation, which appears to be inconsistent with experimental reports to a certain extent.[13] Because the rate of a photocatalytic reaction can be controlled by several steps, the interactions between H_2O and a photocatalyst surface also play a key role during the photocatalytic process. However, the structure–activity relationships associated with the interactions between H_2O and Zn_2GeO_4 surfaces are not fully understood. Therefore, a better understanding of these relationships and active sites on Zn_2GeO_4 surfaces is of fundamental interest and theoretical importance.

It is generally believed that in addition to the effect of morphology and surface microstructure, the chemical properties of perfect surfaces differ markedly from those of surfaces containing oxygen defects.[14] Therefore, oxygen defects are considered to be important reactive agents for many adsorbates, and hence, many surface reactions are influenced by oxygen defects.[12,15−18] In addition to acting as direct active sites, oxygen defects also act as electron donor sites, thus altering the

Received: November 30, 2012
Accepted: July 17, 2013
Published: July 17, 2013

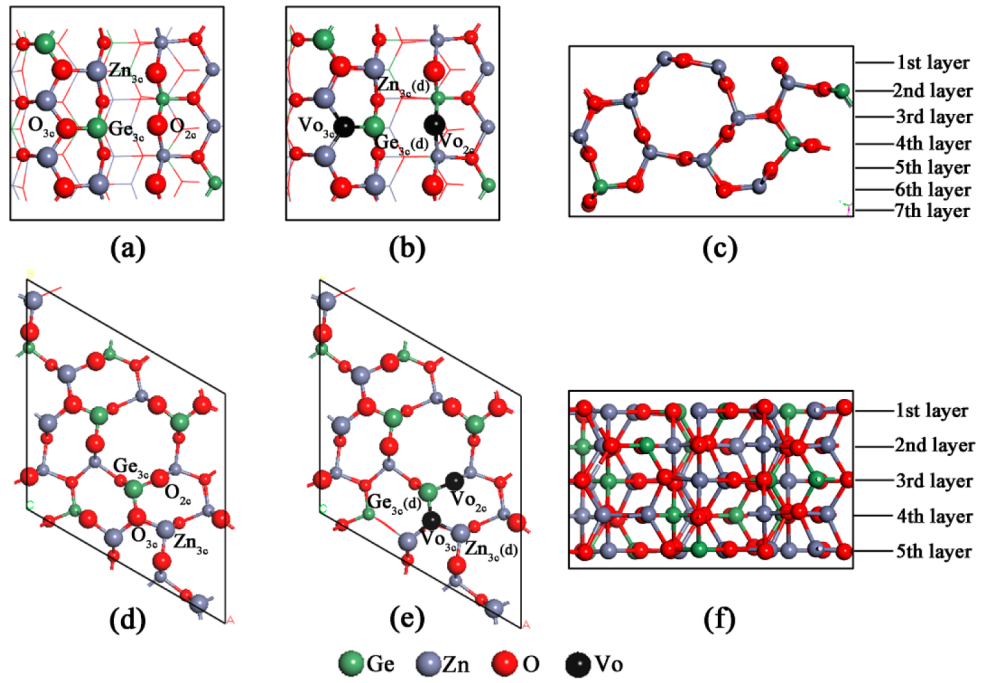

Figure 1. (a) Top view of perfect (010) surface; (b) top view of defective (010) surface; (c) side view of (010) surface; (d) top view of perfect (001) surface; (e) top view of defective (001) surface; and (f) side view of (001) surface.

surface electronic structure.[14,19,20] It is therefore very important to understand the effect of oxygen defects on the interaction of H_2O with photocatalyst surfaces.

In the present work, we employed density functional theory (DFT) to investigate the adsorption of H_2O on Zn_2GeO_4 (010) and (001) surfaces, focusing on the influence of surface structure and oxygen defects on adsorption performance. The energies and geometries of adsorption modes were determined, and detailed analyses of the electronic structure with the local density of states (LDOS) and charge density were carried out. It was found that the interaction of H_2O with perfect Zn_2GeO_4 surfaces was dependent on their structure. On a perfect Zn_2GeO_4 (010) surface, dissociative adsorption was favored. In contrast, on a perfect Zn_2GeO_4 (001) surface, molecular adsorption was more stable. After the introduction of an oxygen defect, dissociative adsorption was the most favorable adsorbate configuration on a defective (010) surface. Moreover, in the case of H_2O adsorption on a defective (001) surface, only molecular adsorption was observed. The result about the adsorbate geometries, catalytic activity of various surface sites, specific electronic structure of surface Ge_{3c} atoms, and their relevance to surface structure will be useful for the future design of the Zn_2GeO_4 photocatalyst, as well as for the atomistic-level understanding of other structure-sensitive reactions. This paper is organized as follows. The computational methods and surface models are described in detail in Section 2, whereas the calculated results are reported and discussed in Section 3. Finally, the most important conclusions are summarized in Section 4.

2. COMPUTATIONAL METHODS AND SURFACE MODELS

DFT[21] with a GGA-PW91[22,23] functional, as implemented in the CASTEP program,[24] was used for all the calculations. The Vanderbilt ultrasoft pseudopotential[25] was used for the treatment of core electrons, and H $1s^1$, O $2s^2$ $2p^4$, Zn $3d^{10}$ $4s^2$, and Ge $4s^2$ $4p^2$ electrons were treated as valence electrons. A plane-wave basis set was used with the cutoff energy set at 340 eV, and this cutoff energy was used throughout our calculations. Monkhorst-Pack[26] grids of 3 × 3 × 3 k-points were used for the bulk unit cell, and grids of 2 × 2 × 1 k-points were used for (010) and (001) surfaces. Our test calculations with Monkhorst-Pack grids of 3 × 2 × 1 and 3 × 3 × 1 k-points gave almost the same geometries and adsorption energies as those obtained using the Monkhorst-Pack grids of 2 × 2 × 1 and 2 × 2 × 1 k-points for (010) and (001) surfaces, respectively. A Fermi smearing of 0.1 eV was used in the calculations.

Previous experimental work[11] has shown that Zn_2GeO_4 nanobelts are uniform single crystals with the longitudinal direction along [001] and the width direction along [100]. The two major exposed surfaces of the nanobelts are {010} facets. In principle, the crystallographic (100) and (010) surfaces of rhombohedral Zn_2GeO_4 are equivalent. Therefore, two surfaces of Zn_2GeO_4—(010) and (001) surfaces—were considered in this work. These surfaces were created on the basis of an optimized bulk unit cell with cell parameters of 14.486 Å × 14.486 Å × 9.656 Å and were modeled using a (1 × 1) supercell with dimensions of 9.656 Å × 14.486 Å × 8.209 Å (seven atomic layers) and 14.486 Å × 14.486 Å × 6.696 Å (five atomic layers). The (001) surface of Zn_2GeO_4 has only one termination mode, exposing 2-fold coordinated O, 3-fold coordinated O, 3-fold coordinated Ge, and 3-fold coordinated Zn. In contrast, the (010) surface of Zn_2GeO_4 has several different terminations, exposing 1-fold coordinated O, 2-fold coordinated O, 3-fold coordinated O, 2-fold coordinated Ge, 3-fold coordinated Ge, 2-fold coordinated Zn, and 3-fold coordinated Zn atoms. In the present work, the (010) surface was terminated by exposing 2-fold coordinated O, 3-fold coordinated O, 3-fold coordinated Ge, and 3-fold coordinated Zn, which is the most favorable cleavage because it breaks only 9 bonds versus 15 or 18 for other cleavages. The vacuum region separating the slabs along the [001] direction was set to 12 Å. The geometry of an isolated H_2O molecule was optimized using a large cell with dimensions of 10 Å × 10 Å × 10 Å. The calculated values of the O−H bond length and H−O−H angle were 0.977 Å and 104.3°, respectively, which were consistent with previously calculated values of 0.979 Å and 104.5°,[27] respectively. In all calculations, the atoms in the bottom layers were fixed, whereas the atoms in the three topmost layers as well as H and O atoms in H_2O were allowed to relax. After optimization, LDOS and

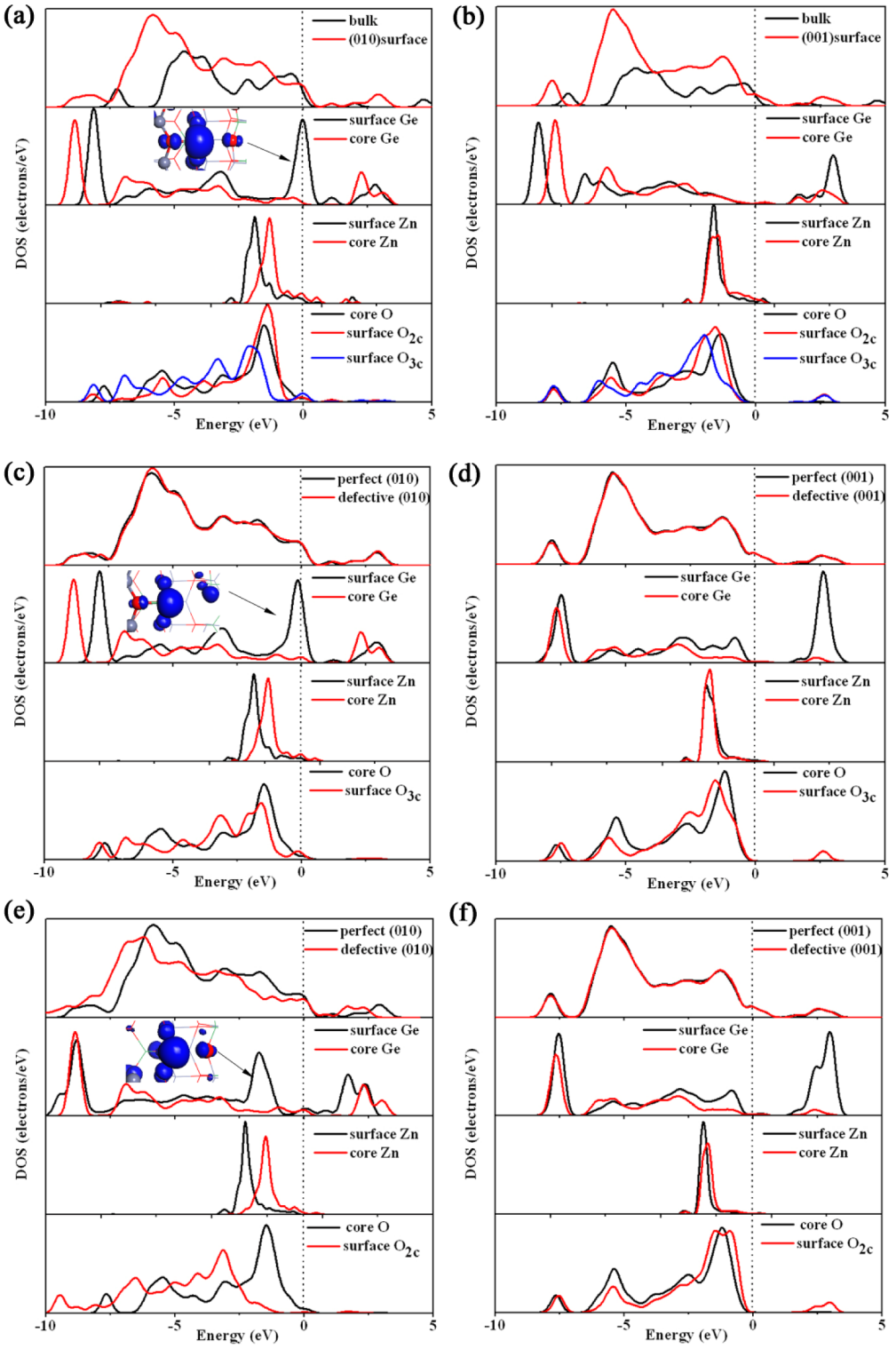

Figure 2. LDOS for (a) perfect Zn_2GeO_4 (010) surface, (b) perfect Zn_2GeO_4 (001) surface, (c) defective Zn_2GeO_4 (010) surface with V_{O2c}, (d) defective Zn_2GeO_4 (001) surface with V_{O2c}, (e) defective Zn_2GeO_4 (010) surface with V_{O3c}, and (f) defective Zn_2GeO_4 (001) surface with V_{O3c}. In panels a, c, and e, 3D distributions of various electronic states for surface states are included as insets. Fermi level is set to zero and marked by a vertical dotted line.

charge density were analyzed. These analyses were used to understand the nature of the bonding and interaction between H_2O and Zn_2GeO_4 surfaces.

Adsorption energy is defined as

$$E_{ads} = E(H_2O/slab) - [E(H_2O) + E(slab)]$$

where the first term denotes the total energy of a slab with H_2O adsorbed on the surface; the second term denotes the total energy of free H_2O; and the third term denotes the total energy of a bare slab surface. According to the above definition, a negative E_{ads} value corresponds to an exothermic adsorption, and a more negative E_{ads} value implies stronger adsorption.

dx.doi.org/10.1021/am4015692 | ACS Appl. Mater. Interfaces 2013, 5, 6893−6901

3. RESULTS AND DISCUSSION

3.1. Geometric and Electronic Structure of Perfect and Defective Zn_2GeO_4 Surfaces. Perfect and defective Zn_2GeO_4 (010) and (001) surfaces have been analyzed in detail in our previous work.[13] Here, a concise introduction to Zn_2GeO_4 (010) and (001) surfaces is provided for easy reference.

In order to establish slab models for Zn_2GeO_4 (010) and (001) surfaces, surface energies were first evaluated using the equation $S = (E^N_{slab} - NE_{bulk})/2A$, where A is the area of the surface, E^N_{slab} is the total energy of surface slabs, N is the number of Zn_2GeO_4 units in the cell, and E_{bulk} is the energy per stoichiometric unit of the bulk. For a slab whose top and bottom surfaces are not equivalent, the surface energy of the slab is given by $S = (E^N_{slab} - NE_{bulk})/A - S_{bottom}$. S_{bottom} was calculated using a slab with identical termination on both sides without any surface relaxation. The calculated surface energies of the (010) surface with a thickness of seven, eight, and nine atomic layers are 2.13, 2.14, and 2.11 J/m^2, respectively. Further, the calculated surface energies of the (001) surface with a thickness of five, seven, and nine atomic layers thickness are 2.66, 2.70, and 2.74 J/m^2, respectively. These results show that the surface energies converged to within 0.01−0.03 J/m^2 for the (010) surface and 0.04−0.08 J/m^2 for the (001) surface, indicating that thicknesses of seven and five layers for the (010) and (001) surfaces, respectively, are enough for the calculated models. Therefore, to keep the computational cost low, we chose only these two slabs to study H_2O adsorption in the present work.

Figure 1a, d show the top view of perfect Zn_2GeO_4 (010) and (001) surfaces, respectively. Perfect Zn_2GeO_4 (010) and (001) surfaces contained 3-fold coordinated Ge (Ge_{3c}), 3-fold coordinated Zn (Zn_{3c}), 3-fold coordinated O (O_{3c}), and 2-fold coordinated O (O_{2c}) sites. The Ge_{3c}, Zn_{3c}, and O_{2c} sites resulted from the 4-fold coordinated Ge (Ge_{4c}), 4-fold coordinated Zn (Zn_{4c}), and 3-fold coordinated O (O_{3c}) atoms of bulk Zn_2GeO_4, respectively, and were therefore coordinately unsaturated. The O_{3c} site was saturated as it resulted from the O_{3c} atom of bulk Zn_2GeO_4. Defective Zn_2GeO_4 (010) and (001) surfaces with an oxygen vacancy (V_O) were created by removing a surface O_{2c} or O_{3c} atom from perfect Zn_2GeO_4 (010) and (001) surfaces. The original Ge_{3c} and Zn_{3c} atoms bound to a top O (O_{2c} or O_{3c}) atom at a vacancy site became 2-fold coordinated and are denoted as Ge_{3c}(d) and Zn_{3c}(d), respectively, as shown in panels b and e in Figure 1. In this figure, the location of V_O is indicated using a black sphere. The V_O formation energy is defined with respect to the energy of an oxygen molecule in the triplet state and is calculated according as $E_{V_o} = -(E_{perfect} - E_{defective} - (1/2)E_{O_2})$. The calculated formation energies for V_{O2c} and V_{O3c} marked on the (010) surface are 3.68 and 3.21 eV, respectively; further, the calculated formation energies for V_{O2c} and V_{O3c} marked on the (001) surface are 2.72 and 3.03 eV, respectively.[13] In addition, Mulliken charge analysis showed that V_O formation was accompanied by the localization of two electrons on nearby Ge and Zn atoms, and the Mulliken charges of perfect and defective Zn_2GeO_4 (010) and (001) surfaces are shown in Figure S1 in the Supporting Information.

The calculated LDOS values for perfect and defective Zn_2GeO_4 (010) and (001) surfaces are shown in Figure 2. For comparison, the LDOS values for bulk Zn_2GeO_4 are also reported. The Fermi level is set to zero and marked by a vertical dotted line. In Figure 2a, a comparison between the LDOS values for surface and core Ge shows the existence of a sharp, strong, and nondispersed band located at the Fermi level, which consists of Ge 4s and 4p states, as shown in the stereopicture in Figure 2a. Moreover, the LDOS values for surface O atoms, which are in the vicinity of surface Ge_{3c} atoms, are also plotted in Figure 2a. The LDOS of surface O_{2c} 2p states show a slight increase, whereas those of surface O_{3c} 2p states show a slight decrease. The presence of O 2p and Ge 4s and 4p states at the Fermi level strongly suggest that these are surface states. Generally, the formation of surface states is due to the presence of dangling bonds on the semiconductor surface; therefore, the quantum states of surface electrons are discrete levels or narrow bands.[28,29] Hence, the presence of coordinately unsaturated surface Ge_{3c} atoms on the (010) surface is the main reason for the existence of surface states, and surface O_{2c} and O_{3c} atoms in the vicinity of surface Ge_{3c} atoms participate to construct the surface states, as shown in the stereopicture in Figure 2a. For the perfect (001) surface, no surface states exist in the bandgap, and the band of surface Ge atoms appears as a broad band within the valence band of core Ge atoms, as shown in Figure 2b. Mulliken charge analysis showed that the charges of surface Ge atoms are 1.09 |e| and 1.49 |e| for (010) and (001) surfaces, respectively. By analyzing the geometric structure of (010) and (001) surfaces, it was found that the difference in the geometric structure around surface Ge atoms led to a difference in the electronic structure.

After introduction of an oxygen defect, the defective (010) surface with V_{O2c} (Figure 2c) is similar to the perfect (010) surface and has a surface state at the Fermi level. For the defective (010) surface with V_{O3c} (Figure 2e), the surface state can be clearly seen at the top of the valence band (about 2 eV below E_F); however, for defective (001) surfaces (with V_{O2c} or V_{O3c}), no surface state exists, as shown in panels d and f in Figure 2. These observations indicate that the presence of V_{O2c} on the (010) surface and V_{O2c} or V_{O3c} on the (001) surface does not significantly modify the electronic structure of Zn_2GeO_4 surfaces, whereas the energy band of surface Ge atoms shows a significant downward shift because of the presence of V_{O3c} on the (010) surface.

3.2. H_2O Adsorption on Perfect Zn_2GeO_4 Surfaces. H_2O molecule can interact with the Zn_2GeO_4 surfaces via several different ways by utilizing H atoms and O lone-pair electrons (Figure 3). For clarity, the oxygen and hydrogen

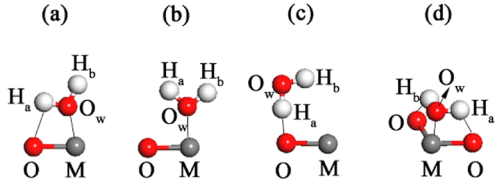

Figure 3. Possible configurations for H_2O molecule adsorbed on Zn_2GeO_4 surface (M = Zn or Ge).

atoms of H_2O are denoted as O_w and H_a and H_b, respectively. We optimized different H_2O adsorption models and obtained the adsorption energy for each structure. Here, we discuss only the most energetically favorable structures.

We start the discussion with H_2O molecule on the perfect Zn_2GeO_4 (010) surface. The adsorbate geometries and key structural parameters are shown in Figure 4. These include dissociative adsorption at the $Ge_{3c}\cdots O_{2c}$ site and molecular

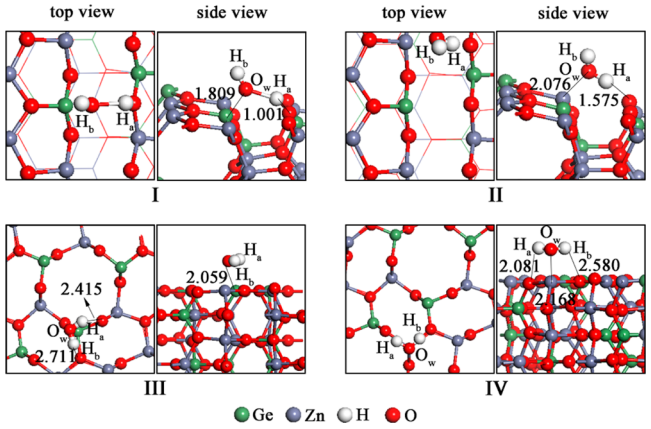

Figure 4. Optimized stable configurations for H_2O adsorption on perfect Zn_2GeO_4 (010) and (001) surfaces. Distances are given in Å.

adsorption at the $Zn_{3c}\cdots O_{2c}$ site, as shown in Figure 4. We denote these configurations as I and II, respectively. Further, the adsorption energies for dissociative and molecular adsorption were calculated to be −2.30 and −1.21 eV (Table 1), respectively. Clearly, the dissociative adsorption of H_2O is

Table 1. Structural Parameters and Adsorption Energies for Isolated H_2O Molecule and Different H_2O Adsorption Configurations on Perfect and Defective Zn_2GeO_4 Surfaces

configurations	O_w−H_a bond (Å)	O_w−H_b bond (Å)	H_a−O_w−H_b angle (deg)	E_{ads} (eV)
I	1.766	0.977	134.9	−2.30
II	1.030	0.975	110.0	−1.21
III	1.073	0.985	108.7	−0.89
IV	1.009	0.981	115.9	−0.65
D-I	2.987	0.980	66.7	−2.40
D-II	1.913	0.979	132.7	−2.35
D-III	2.951	0.977	66.0	−1.68
D-IV	1.744	0.977	128.4	−1.38
D-V	1.058	0.975	109.9	−1.63
D-VI	0.986	0.978	109.2	−0.66
H_2O molecule	0.977	0.977	104.3	--

energetically more favorable than the molecular one. For dissociative adsorption, one of the H_2O decomposition products—O_wH_b group—is adsorbed onto the Ge_{3c} atom with its O_w atom bonded to the Ge_{3c} atom, thus forming a surface-adsorbed hydroxyl radical.[27] The other H_2O decomposition product—H_a atom—is adsorbed onto the O_{2c} atom, which interacts with the Ge_{3c} atom. Thus, it becomes a stable surface-terminated hydroxyl radical.[27] The distances of the newly formed O_w−Ge_{3c} and H_a−O_{2c} bonds are 1.809 and 1.001 Å, respectively. The molecular plane of dissociated H_2O is approximately perpendicular to the surface. In addition, H_2O binding in the molecular form is unstable at the $Ge_{3c}\cdots O_{2c}$ site with zero barriers for dissociation (see the potential energy profile in the Supporting Information Figure S2). In the case of molecular adsorption, the O_w atom interacts with the Zn_{3c} atom, with the H_a atom pointing toward the neighboring O_{2c} atom. The distances of the newly formed O_w−Zn_{3c} and H_a−O_{2c} bonds are 2.076 and 1.575 Å, respectively. The molecular plane of H_2O is approximately perpendicular to the surface when H_2O is adsorbed at this site. The detailed structural parameters are listed in Table 1.

Next, H_2O adsorption on the perfect Zn_2GeO_4 (001) surface was studied. Two stable molecular adsorption configurations—denoted as III and IV—were obtained (see Figure 4) for this adsorption. The optimized structures and key structural parameters are given in Figure 4, and the adsorption energies (E_{ads}) as well as other structural parameters of these configurations are listed in Table 1. The stable sites for molecular adsorption are O_{2c}−Ge_{3c}−O_{3c} and O_{2c}−Zn_{3c}−O_{3c} sites. The molecular plane of H_2O is approximately parallel to the Zn_2GeO_4 (001) surface when H_2O is adsorbed at these sites. For these molecular adsorption configurations, the O_w atom of H_2O interacts with the Ge_{3c} or Zn_{3c} atoms, with the two H atoms pointing toward neighboring O_{2c} and O_{3c} atoms. The distances of the newly formed O_w−Ge_{3c} and O_w−Zn_{3c} bonds in III and IV are 2.059 and 2.168 Å, respectively. The calculated H_2O adsorption energies for these sites are −0.89 and −0.65 eV, respectively.

Generally, the adsorbate−surface interaction is mainly local in character.[30] Therefore, the analysis of LDOS and electron charge density for H_2O−Zn_2GeO_4 should provide at least a qualitative insight into the bonding interaction of H_2O with Zn_2GeO_4 surfaces. Figures 5a−d shows the LDOS and charge

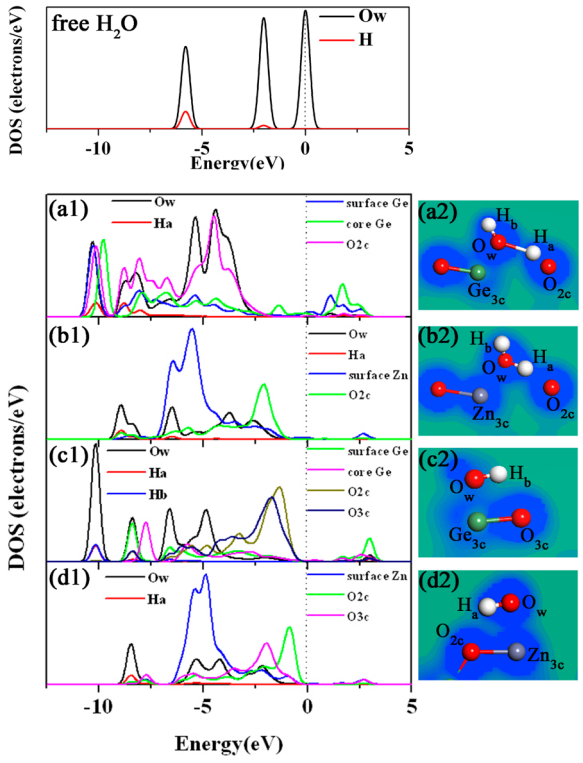

Figure 5. LDOS and charge density plots for H_2O adsorption on perfect Zn_2GeO_4 (010) and (001) surfaces: (a) configuration I, (b) configuration II, (c) configuration III, and (d) configuration IV. For charge density plots, a plane parallel to B and C axes of slab was used for cross-section. Fermi level is set to zero and marked by a vertical dotted line.

density plots for configurations I, II, III, and IV, respectively. For dissociative adsorption configuration I, the O_w atom strongly interacts with the unsaturated surface Ge_{3c} atom, the H_a atom interacts with the surface O_{2c} atom, and the hybridization effect is clearly observed in the energy range from −11 to −2.5 eV. The corresponding states completely overlap, and their positions and shapes change. The changes in

dx.doi.org/10.1021/am4015692 | ACS Appl. Mater. Interfaces 2013, 5, 6893−6901

the electronic structure indicate that the interaction of H_2O with the (010) surface is strong in the dissociative adsorption state. This interaction is also evidenced by the charge density plots shown in Figure 5a2. For molecular adsorption, the overlap of corresponding states is partial. In configuration II, the interaction of H_2O with the (010) surface is mainly dependent on the hybridization of its lone pairs of electrons with surface Zn_{3c} 3d states, and that of H_a 1s states with surface O_{2c} 2p states, as shown in Figure 5b. In configuration III, H_2O mainly interacts with the (001) surface via the hybridization of its orbitals with surface Ge_{3c} and O 2p orbitals, as shown in Figure 5c. In configuration IV, the interaction of H_2O with the (001) surface is mainly dependent on the hybridization of H_2O orbitals with surface Zn_{3c} 3d and O 2p orbitals. As shown in Figure 5d2, Zn_{3c} forms small hybridization with the O_w atom.

The above results show that the interaction of H_2O with Zn_2GeO_4 surfaces is strongly dependent on the surface structure. From the interaction energies presented in Table 1, it is clear that the adsorption of H_2O on the (010) surface is more stable than that on the (001) surface. Moreover, the interaction between H_2O and the (010) surface results in a dissociative adsorption mode. This requires the presence of a $Ge_{3c}\cdots O_{2c}$ site to interact with the H and O atoms of H_2O.

3.3. H_2O Adsorption on Defective Zn_2GeO_4 Surfaces.

In metal oxide surfaces, oxygen defects play an important role and can significantly influence the interaction of H_2O with the surfaces. In this study, we investigated the adsorption of H_2O on defective Zn_2GeO_4 surfaces at or near V_O. We first considered H_2O adsorption on the defective Zn_2GeO_4 (010) surface with V_{O2c}. As in the case of the perfect surface, we explored different H_2O adsorption structures and the favorable adsorbate configurations are shown in Figure 6. We denote these configurations as D-I and D-II. Both the favorable adsorbate configurations on the defective Zn_2GeO_4 (010) surface with V_{O2c} correspond to dissociative adsorption. The adsorption energy values and structural parameters are listed in Table 1. In configuration D-I, H_2O is adsorbed at the V_{O2c} site and dissociates into an O_wH_b group that fills the oxygen vacancy, and a H_a atom that bonds to surface Ge_{3c} atom with an adsorption energy of −2.40 eV. The distance of the newly formed H_a-Ge_{3c} bond is 1.528 Å. In addition, H_2O binding in the molecular form is unstable at the V_{O2c} site with zero barriers for dissociation (see the potential energy profile in the Supporting Information, Figure S3). In configuration D-II, the adsorption of H_2O occurs near the V_{O2c} site with an adsorption energy of −2.35 eV. The distances of the newly formed O_w-Ge_{3c} and H_a-O_{2c} bonds are 1.806 Å and 0.992 Å, respectively. Therefore, when V_{O2c} is created on the (010) surface, the adsorption energies are generally greater than those in the case of the perfect surface, indicating an effective attraction between H_2O and V_O.

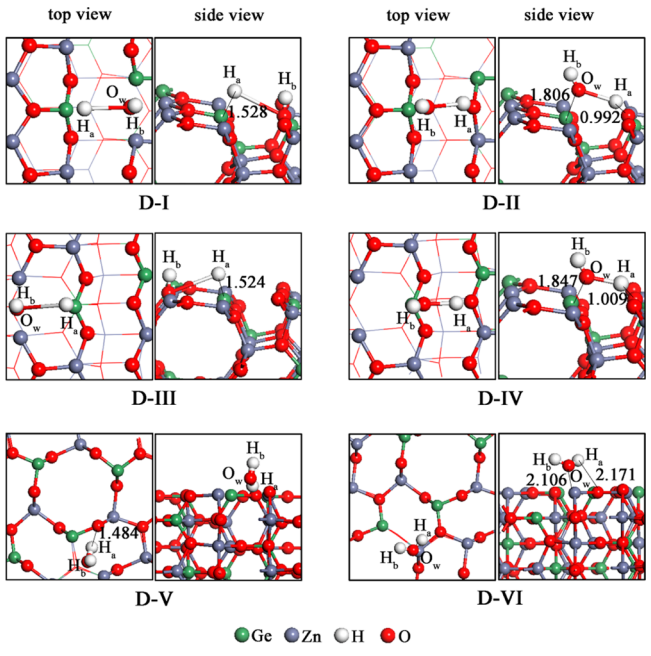

Figure 6. Optimized stable configurations for H_2O adsorption on defective Zn_2GeO_4 (010) and (001) surfaces. Distances are given in Å.

We then investigated H_2O adsorption on the defective Zn_2GeO_4 (010) surface with V_{O3c}. Different adsorption configurations in the presence of V_{O3c} were examined, and the favorable adsorbate configurations—denoted as D-III and D-IV—are shown in Figure 6. As shown in this figure, both favorable configurations for H_2O adsorption on the defective Zn_2GeO_4 (010) surface with V_{O3c} correspond to dissociative adsorption. In configuration D-III, H_2O is adsorbed at the surface V_{O3c} site and dissociates into an O_wH_b group that fills the oxygen vacancy and a H_a atom that bonds to surface Ge_{3c} atom with an adsorption energy of −1.68 eV. In configuration D-IV, H_2O adsorption occurs near the V_{O3c} site with an adsorption energy of −1.38 eV. The above results show that the presence of a surface vacancy on the (010) surface has a dual effect on the adsorption properties of H_2O. First, it modifies the adsorption energy for those configurations in which H_2O adsorption on the perfect (010) surface occurs at sites near the vacancy. Second, it leads to the creation of new dissociative adsorption configurations at the V_O site that are not obtained on the perfect (010) surface. These results are consistent with previous reports suggesting the existence of attraction between H_2O and V_O. Fronzi et al.[17] analyzed H_2O adsorption on stoichiometric and reduced CeO_2 (111) surfaces and found that an effective attractive interaction exists between H_2O and V_O. Mulakaluri et al.[31] investigated the adsorption of H_2O on a Fe_3O_4 (001) surface and found that oxygen defects strongly promote H_2O dissociation.

Next, we considered the adsorption of H_2O on the defective Zn_2GeO_4 (001) surface with V_O. Different H_2O adsorption structures on the defective Zn_2GeO_4 (001) surface were examined, and the two most stable configurations were identified (Figure 6). These configurations are denoted as D-V and D-VI. For D-V and D-VI, the calculated adsorption energies for H_2O adsorption in the vicinity of V_O sites are −1.63 and −0.66 eV, respectively. In configuration D-V, H_2O is adsorbed near the V_{O3c} site and interacts with the defective (001) surface through the formation of a H_a-O_{2c} hydrogen bond. The molecular plane of H_2O is approximately vertical to the surface. In configuration D-VI, H_2O is adsorbed near the V_{O2c} site and interacts with the defective (001) surface through the formation of an O_w-Zn_{3c}(d) bond and a H_a-O_{2c} hydrogen bond. In this case, however, the molecular plane of H_2O is approximately parallel to the surface. This indicates that the presence of surface V_O can modify the energy for the adsorption of H_2O on the perfect (001) surface but cannot change its adsorbed form.

To further investigate the interaction between adsorbed H_2O and the defective Zn_2GeO_4 surface, the LDOS and charge density for the different configurations were studied. In Figure

7a–f, the LDOS and charge density plots for configurations D-I, D-II, D-III, D-IV, D-V, and D-VI, respectively, are shown. For

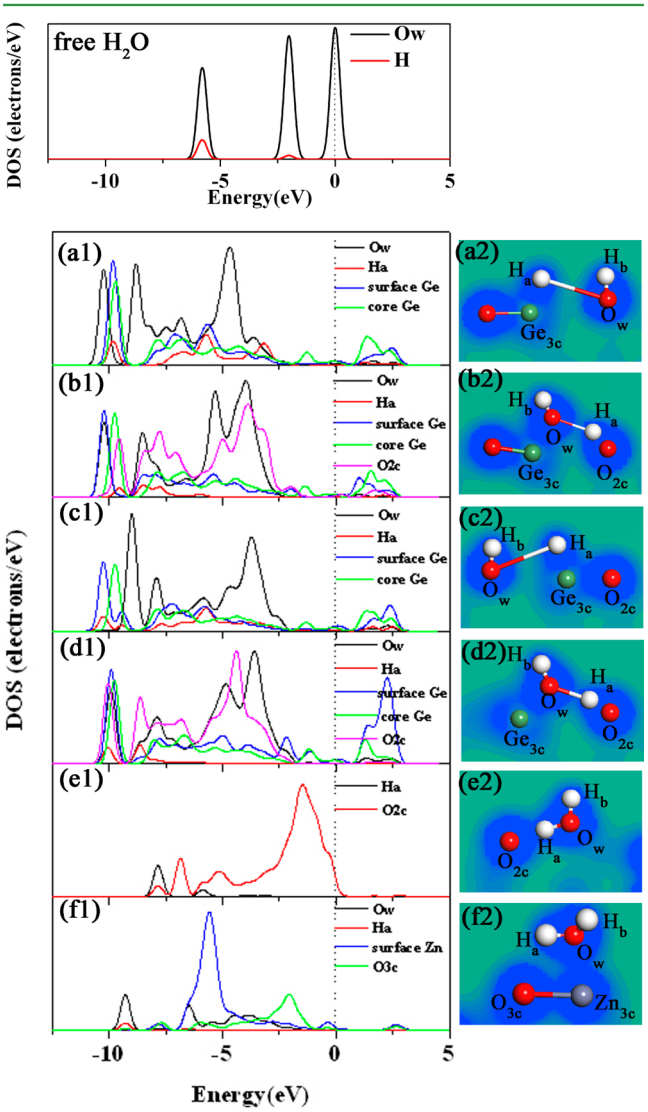

Figure 7. LDOS and charge density plots for H_2O adsorption on defective Zn_2GeO_4 (010) and (001) surfaces: (a) configuration D-I, (b) configuration D-II, (c) configuration D-III, (d) configuration D-IV, (e) configuration D-V, and (f) configuration D-VI. For charge density plots, a plane parallel to the B and C axes of slab was used for cross-section. Fermi level is set to zero and marked by a vertical dotted line.

configurations D-I and D-III, in which H_2O is adsorbed directly at the V_O site, the O_wH_b group fills V_O and the H_a atom is bonded to the surface Ge_{3c} atom. Thus, there is a clear hybridization between the surface Ge_{3c} orbital and H_2O orbitals, as shown in panels a and c in Figure 7. For configurations D-II and D-IV, in which H_2O is adsorbed near the V_O site, the O_wH_b group is bonded to the surface Ge_{3c} atom and the H_a atom is bonded to the surface O_{2c} atom. For these configurations, hybridization is more obvious in the energy range from −11 to −2.5 eV because of the stronger interaction of the O_w and H_a atoms with the surface Ge_{3c} and O_{2c} atoms, as shown in panels b and d in Figure 7, whereas for the configurations D-V and D-VI, the hybridization between the orbitals of the H_a or O_w and surface O or Zn_{3c} atoms is relatively weak, as shown in panels e and f Figure 7.

The above results show that the interaction of H_2O with defective Zn_2GeO_4 surfaces is dependent on the surface structure: the adsorption ability of H_2O for the defective (010) surface is generally higher than that for the defective (001) surface. Moreover, all favorable configurations for H_2O adsorption on the defective (010) surface corresponded to dissociative adsorption, whereas all favorable configurations for H_2O adsorption on the defective (001) surface corresponded to molecular adsorption. Furthermore, the presence of surface vacancies can modify the energies for the adsorption of H_2O on perfect surfaces.

3.4. General Discussion. We carried out a detailed analysis of the interaction of H_2O with the perfect and defective Zn_2GeO_4 (010) and (001) surfaces by using DFT calculations. Our calculations showed that the interaction of H_2O with Zn_2GeO_4 surfaces is strongly dependent on the surface structure. For perfect and defective (010) surfaces, we found the interaction between H_2O and surfaces to be strong, and that this interaction leads to a dissociative adsorption mode. However, for perfect and defective (001) surfaces, we found the interaction between H_2O and surfaces to be weak, and that this interaction leads to a molecular adsorption mode. The origin of the surface dependence can be understood by considering the different surface structures and surface sites. As shown in the present study, for the perfect Zn_2GeO_4 (010) surface, H_2O adsorbed at the $Ge_{3c}\cdots O_{2c}$ site can spontaneously dissociate into an H atom and an OH group, and H_2O adsorbed at the $Zn_{3c}\cdots O_{2c}$ site can lead to large adsorption energy. However, no dissociation is observed over the perfect Zn_2GeO_4 (001) surface. We can therefore conclude that the $M_{3c}\cdots O_{2c}$ structure on the perfect Zn_2GeO_4 (010) surface plays a critical role in the activation of H_2O, and the $Ge_{3c}\cdots O_{2c}$ site is a specific surface site that promotes H_2O dissociation.

We now explain why the $Ge_{3c}\cdots O_{2c}$ site on the perfect Zn_2GeO_4 (010) surface has a superior ability for H_2O bonding. For this, we consider surface electronic structures with and without adsorbed H_2O. By combining the results of H_2O adsorption on perfect and defective Zn_2GeO_4 (010) and (001) surfaces, we mapped out the interaction between H_2O and surface Ge atoms on these surfaces. The results are schematically shown in Figure 8. In Figure 2a, for the perfect (010) surface, the LDOS plot for surface Ge atoms exhibits a specific surface state at the Fermi level, which consists of Ge 4s and 4p states. By comparing Figures 2a and 5a, it can be observed that upon H_2O dissociation, the surface Ge band has a large downshift toward the valence band. This is because the O_wH_b group resulting from the dissociation of H_2O can attach to surface Ge atoms, forming a Ge–O_w bond. The formation of this bond significantly decreases the energy of the Ge band. This large decrease in energy can act as an effective H_2O dissociation agent (see Figure 8a). In Figure 2b, it can be observed that no surface state at the Fermi level exists for the perfect (001) surface, and the band of surface Ge atoms appears as a broad band within the valence band of core Ge atoms. Upon H_2O adsorption, the variations in the band of surface Ge atoms is much more moderate (compare Figures 2b and 5c); thus, H_2O is likely to remain in the molecular form (see Figure 8b). The above analysis shows that the most important factor determining the dissociation of H_2O on Zn_2GeO_4 surfaces is the position of the surface Ge band relative to the Fermi level. This result agrees well with those obtained in previous studies.

dx.doi.org/10.1021/am4015692 | ACS Appl. Mater. Interfaces 2013, 5, 6893–6901

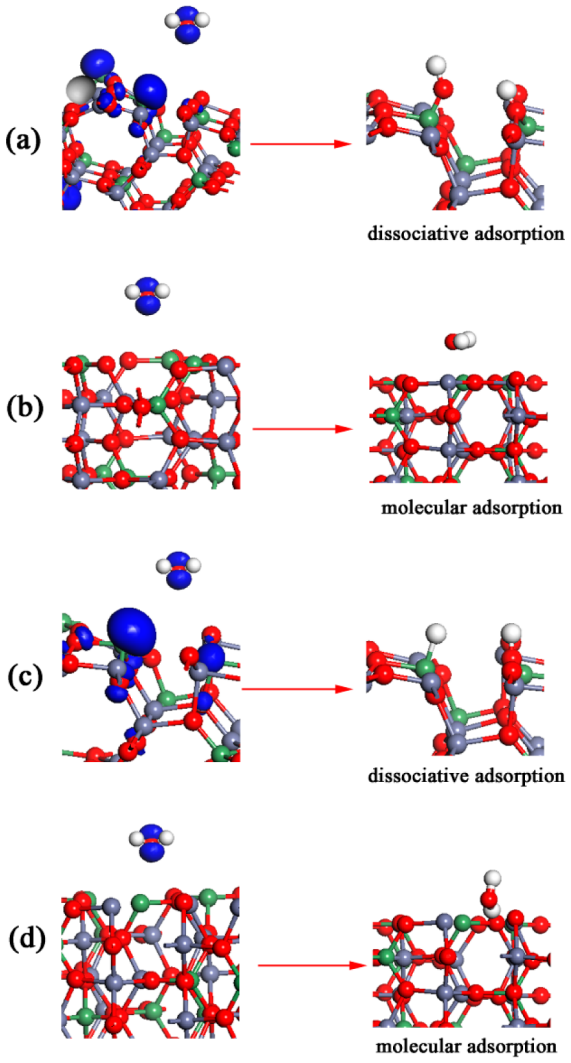

Figure 8. Schematic of interaction between H_2O and surface Ge atoms on (a) perfect (010) surface; (b) perfect (001) surface; (c) defective (010) surface; and (d) defective (001) surface.

Hammer et al.[32] analyzed the structure sensitivity of CO adsorption on different Pt surfaces and found that higher the d band center of surface Pt atoms, the stronger the CO bonding energy. Xu et al.[33] used DFT calculations to study H_2O adsorption on three metal oxide surfaces and found that the position of the surface O 2p level relative to the top of the valence band is an important factor affecting H_2O dissociation on the surface. Hadidi et al.[29] analyzed the fundamental properties of pure and hydrogen-covered (010), (101), (100), and (001) surfaces of $LaNbO_4$ and found that surface states located in the bandgap of the (101) surface contributed toward increasing the reactivity of the surface.

After introduction of V_O, behavior of defective Zn_2GeO_4 surfaces becomes similar to that of perfect Zn_2GeO_4 surfaces, as shown in Figures 2 and 7. For the defective (010) surface with a V_{O2c} site, whose surface Ge band has no significant change compared to perfect (010) surface and has a surface state at the Fermi level (Figure 2c), the O_wH_b group or H_a atom resulting from the dissociation of H_2O can attach to the surface Ge atoms, forming the Ge−O_w or Ge−H_a bond, respectively. The formation of these new bonds greatly reduces the energy of the Ge band. This large decrease in energy can drive H_2O dissociation (see Figure 8c). For the defective (010) surface with a V_{O3c} site, the energy band of surface Ge atoms shows a significant downward shift compared to perfect (010) surface (about 2 eV below E_F, as shown in Figure 2e), the O_wH_b group or H_a atom resulting from the dissociation of H_2O can attach to the surface Ge atoms, forming the Ge−O_w or Ge−H_a bond, respectively. Therefore, H_2O can still be dissociated; however, because of the significant reduction in the energy of the surface Ge band, the adsorption energy becomes significantly lower than that in the case of H_2O adsorption with the V_{O2c} site. Moreover, for the defective (001) surface, no interaction exists between H_2O and surface Ge atoms because no surface state exists (Figure 8d). These results show that the surface state is an important factor affecting H_2O dissociation on Zn_2GeO_4 surfaces, and the difference in the location of the surface state relative to the Fermi level has a strong effect on the adsorption energies of H_2O.

In summary, the results obtained in this study show that H_2O adsorption on Zn_2GeO_4 surfaces can be concisely described in terms of molecular orbitals: the coupling between adsorbate levels and the electrons of surface metal (Ge or Zn) or oxygen leads to new adsorbate levels and greatly reduces the energy of the surface metal or oxygen band level. For the perfect and defective (010) surfaces, the energy shift is large because they have a specific surface state at the top of the valence band; this large energy shift can drive H_2O dissociation. In general, a catalytic reaction consists of adsorption, dissociation, recombination, and desorption processes, and for metal or metal oxide catalysts, the results presented above indicate that the adsorption or dissociation of small molecules on the catalyst surface greatly depends on the position of the surface state. These results can be generalized to other adsorbates and provide a conceptual basis for understanding other surface reactions. Moreover, in combination with the results of our previous work,[13] it was found that the activation of CO_2 and dissociation of H_2O occur on different surfaces: the dissociation of H_2O occurs on the major exposed surface (010), while the (001) surface has higher ability for CO_2 activation. These results suggest that for the photocatalytic reduction of CO_2 to CH_4 over Zn_2GeO_4 nanobelts, a simple synthesis of a photocatalyst with exposed specific facets as major surfaces cannot achieve the highest catalytic efficiency. Thus, in future experimental studies, the morphology of Zn_2GeO_4 nanobelts should be optimized and nanobelts with an appropriate proportion of exposed (010) and (001) surfaces should be synthesized for achieving the highest catalytic efficiencies.

4. CONCLUSIONS

In this work, we employed DFT to investigate the adsorption of H_2O on Zn_2GeO_4 (010) and (001) surfaces, focusing on the influence of surface structure and oxygen defects on adsorption performance. The energies and geometries of adsorption modes were calculated and detailed analyses of the electronic structure with LDOS and charge density were carried out. The main findings are as follows:

(1) For the perfect Zn_2GeO_4 (010) surface, a surface state located at the Fermi level exists. However, for the perfect (001) surface, no surface state exists. The presence of V_{O3c} can significantly modify the electronic structure of the Zn_2GeO_4 (010) surface.

(2) The ability of the perfect (010) surface for H_2O adsorption is higher than that of the perfect (001)

surface. On the perfect (010) surface, dissociative adsorption is favored, the $Ge_{3c}\cdots O_{2c}$ site strengthens the H_2O-surface adsorption bond, and H_2O can spontaneously dissociate into a H atom and an OH group. In contrast, on the perfect (001) surface, molecular adsorption is favored, and the stable sites for molecular adsorption are the $O_{2c}-Ge_{3c}-O_{3c}$ and $O_{2c}-Zn_{3c}-O_{3c}$ sites. We have identified the surface state at the Fermi level to be an important factor affecting H_2O dissociation on the (010) surface.

(3) The most favorable adsorbate configurations on the defective (010) surface all correspond to dissociative adsorption; however, for H_2O adsorption on the defective (001) surface, only molecular adsorption is observed. The presence of a surface vacancy can modify the energies for the adsorption of H_2O on the perfect surface; moreover, the value of adsorption energies greatly depends on the position of the surface state.

(4) The dissociation products of H_2O on the perfect (010) surface result in two types of surface hydroxyl radicals. One is the surface-adsorbed hydroxyl radical, which results from the O_wH_b group, in which the O_w atom bonds with the unsaturated surface Ge_{3c} atom and its H_b atom points away from the surface. The other is the stable surface-terminated hydroxyl radical, which results from the H_a atom adsorbed on the unsaturated surface O_{2c} atom.

In summary, our results demonstrate that the interaction of H_2O with Zn_2GeO_4 surfaces is structure sensitive, and that the surface state at the top of the valence band on the (010) surface is the fundamental reason for H_2O dissociation. The information about the adsorbate geometries, catalytic activity of various surface sites, specific electronic structure of surface Ge_{3c} atoms, and their relevance to surface structure will be useful for the future design of the Zn_2GeO_4 photocatalyst, as well as for the atomistic-level understanding of other structure-sensitive reactions.

■ ASSOCIATED CONTENT

Supporting Information

The Mulliken charges of perfect and defective Zn_2GeO_4 (010) and (001) surfaces; potential energy profile of H_2O dissociation on perfect and defective Zn_2GeO_4 (010) surfaces; and processes of H_2O molecule adsorption on perfect and defective Zn_2GeO_4 (010) and (001) surfaces in the form of a movie clip. This material is available free of charge via the Internet at http://pubs.acs.org/.

■ AUTHOR INFORMATION

Corresponding Author

*E-mail: fwl@sdu.edu.cn. Tel: 86-531-88366330. Fax: 86-531-88364864.

Notes

The authors declare no competing financial interest.

■ ACKNOWLEDGMENTS

This work was supported by the National Natural Science Foundation of China (Grants 51172127, 21173131, and 91022034), Excellent Youth Foundation of Shandong Scientific Committee (Grant JQ201015), the 973 Program of China (Grant 2009CB930103), and Independent Innovation Foundation of Shandong University (Grant 2012TS212).

■ REFERENCES

(1) Tong, H.; Ouyang, S. X.; Bi, Y. P.; Umezawa, N.; Oshikiri, M.; Ye, J. H. *Adv. Mater.* **2012**, *24*, 229−251.
(2) Hoffmann, M. R.; Martin, S. T.; Choi, W.; Bahnemann, D. W. *Chem. Rev.* **1995**, *95*, 69−96.
(3) Xie, Y. P.; Liu, G.; Yin, L. C.; Cheng, H. M. *J. Mater. Chem.* **2012**, *22*, 6746−6751.
(4) Wu, N. Q.; Wang, J.; Tafen, D. N.; Wang, H.; Zheng, J. G.; Lewis, J. P.; Liu, X. G.; Leonard, S. S.; Manivannan, A. *J. Am. Chem. Soc.* **2010**, *132*, 6679−6685.
(5) Liu, G.; Yu, J. C.; Lu, G. Q.; Cheng, H. M. *Chem. Commum.* **2011**, *47*, 6763−6783.
(6) Zhou, K. B.; Li, Y. D. *Angew. Chem., Int. Ed.* **2012**, *51*, 602−613.
(7) Mor, G. K.; Shankar, K.; Paulose, M.; Varghese, O. K.; Grimes, C. A. *Nano Lett.* **2005**, *5*, 191−195.
(8) Cho, I. S.; Lee, S. W.; Noh, J. H.; Kim, D. W.; Lee, D. K.; Jung, H. S.; Kim, D. W.; Hong, K. S. *J. Mater. Chem.* **2010**, *20*, 3979−3983.
(9) Zhou, Y.; Tian, Z. P.; Zhao, Z. Y.; Liu, Q.; Kou, J. H.; Chen, X. Y.; Gao, J.; Yan, S. C.; Zou, Z. G. *ACS Appl. Mater. Interfaces* **2011**, *3*, 3594−3601.
(10) Yan, S. C; Wan, L. J; Li, Z. S; Zou, Z. G. *Chem. Commun.* **2011**, 5632−5634.
(11) Liu, Q.; Zhou, Y.; Kou, J. H.; Chen, X. Y.; Tian, Z. P.; Gao, J.; Yan, S. C.; Zou, Z. G. *J. Am. Chem. Soc.* **2010**, *132*, 14385−1487.
(12) He, H. Y.; Zapol, P.; Curtiss, L. A. *J. Phys. Chem. C* **2010**, *114*, 21474−21481.
(13) Liu, L.; Fan, W. L.; Zhao, X.; Sun, H. G.; Li, P.; Sun, L. M. *Langmuir* **2012**, *28*, 10415−10424.
(14) Wendt, S.; Schaub, R.; Matthiesen, J.; Vestergaard, E. K.; Wahlstrom, E.; Rasmussen, M. D.; Thostrup, P.; Molina, L. M.; Laegsgaard, E.; Stensgaard, I.; Hammer, B.; Besenbacher, F. *Surf. Sci.* **2005**, *598*, 226−245.
(15) Indrakanti, V. P.; Kubicki, J. D.; Schobert, H. H. *Fuel Process. Technol.* **2011**, *92*, 805−811.
(16) Pipornpong, W.; Wanbayor, R.; Ruangpornvisuti, V. *Appl. Surf. Sci.* **2011**, *257*, 10322−10328.
(17) Fronzi, M.; Piccinin, S.; Delley, B.; Traversa, E.; Stampfl, C. *Phys. Chem. Chem. Phys.* **2009**, *11*, 9188−9199.
(18) Sun, C. H.; Liao, T.; Lu, G. Q.; Smith, S. C. *J. Phys. Chem. C* **2012**, *116*, 2477−2482.
(19) Schaub, R.; Thostrup, P.; Lopez, N.; Laegsgaard, E.; Stensgaard, I.; Norskov, J. K.; Besenbacher, F. *Phys. Rev. Lett.* **2001**, *87*, 266104−1−4.
(20) Linsebigler, A. L.; Lu, G. Q.; Yates, J. T. *Chem. Rev.* **1995**, *95*, 735−758.
(21) Payne, M. C.; Teter, M. P.; Allan, D. C.; Arias, T. A.; Joannopoulos, J. D. *Rev. Mod. Phys.* **1992**, *64*, 1045−1097.
(22) Perdew, J. P.; Chevary, J. A.; Vosko, S. H.; Jackson, A. K.; Pederson, R. M.; Singh, D. J.; Fiolhais, C. *Phys. Rev. B* **1992**, *46*, 6671−6687.
(23) Perdew, J. P.; Wang, Y. *Phys. Rev. B* **1992**, *45*, 13244−13249.
(24) Segall, M.; Lindan, P.; Probert, M.; Pickard, C.; Hasnip, P.; Clark, S.; Payne, M. *J. Phys.: Condens. Matter* **2002**, *14*, 2717−2744.
(25) Vanderbilt, D. *Phys. Rev. B* **1990**, *41*, 7892−7895.
(26) Monkhorst, H. J.; Pack, J. D. *Phys. Rev. B* **1976**, *13*, 5188−5192.
(27) Zhao, Z. Y.; Li, Z. S.; Zou, Z. G. *J. Phys. Chem. C* **2012**, *116*, 7430−7441.
(28) Indrakanti, V. P.; Kubicki, J. D.; Schobert, H. H. *Energy Environ. Sci.* **2009**, *2*, 745−758.
(29) Hadidi, K.; Hancke, R.; Norby, T.; Gunnaes, A. E.; Lovvik, O. M. *Int. J. Hydrogen Energy* **2012**, *37*, 6674−6685.
(30) Zhao, Z. Y.; Li, Z. S.; Zou, Z. G. *J. Phys. Chem. C* **2012**, *116*, 11054−11061.
(31) Mulakaluri, N.; Pentcheva, R.; Scheffler, M. *J. Phys. Chem. C* **2010**, *114*, 11148−11156.
(32) Hammer, B.; Nielsen, O. H.; Norskov, J. K. *Catal. Lett.* **1997**, *46*, 31−35.
(33) Xu, H.; Zhang, R. Q.; Ng, A. M. C.; Djurisic, A. B.; Chan, H. T.; Chan, W. K.; Tong, S. Y. *J. Phys. Chem. C* **2011**, *115*, 19710−19715.